

# An Investigation of Earth and Sea-Return Impedances of Power Electrical Cables

F. A. Uribe, O. Ramos-Leaños and Pavel Zuniga

**Abstract**—This paper investigates the numerical performance of the Wedepohl series and of the Gauss-Kronrod quadrature to calculate ground- and sea-return impedances of power cables. Many computational routines to calculate ground-return impedances of cables used in EMTP-type programs have been proposed without technical justification of their application range. In this paper, we explore the convergence and accuracy of the Wedepohl series based on the number of terms in the series and as a ratio test. As a result, an accurate and stable numerical algorithm to compute ground- and sea-return impedances is proposed. The proposed method is capable of accounting for very low resistivity values and large depths.

**Index Terms**— Offshore transmission system, power cables, time-domain transient response, sea-return impedances.

## I. INTRODUCTION

THE growing necessity of electrical energy surpasses current global production [1]. For this reason, integration of new energy resources such as offshore wind and photovoltaic are of paramount importance. Today, there are many ongoing and future projects to electrically connect countries or islands to the mainland via undersea cables. An example of this is the case of the longest undersea electrical link connecting Morocco to the United Kingdom through a 3,800 km cable, sending 3.6 GW of power coming from solar and eolic sources. In México, there is a new cable link project of 30.4 km to provide electrical energy from Playa del Carmen to Isla Cozumel feeding three lines of 115 kV to provide power for more than eighty thousand inhabitants. The increasing number of undersea power energy transmission projects makes the computation of ground- or sea-return impedances of extreme technical importance.

New formulations to compute earth-return impedance have been recently proposed [2-5] to extend its valid range. However, Pollaczek-Sunde's approximation to the earth-return impedance remains valid for transient analysis of up to 10 MHz; this range includes switching transients which are the main concern when realizing interconnection analysis.

In [6] Wedepohl presented a solution to the Pollaczek-Sunde's integral through a set of low-frequency infinite series tied to a closed-form approximation. This formulation is valid for high frequencies up to 100 kHz for cables buried in the same

trench [6]. A critical frequency cut-off of  $|D/p| < 0.25$  (where  $D$  is depicted in Fig. 1 and  $p$  is the Skin-Effect layer thickness) was also proposed to switch between the series solution and the closed-form approximation [6]. To the best of the authors' knowledge, an efficient solution of the Wedepohl series has not yet been implemented nor included in any commercial EMTP-type software. Even more, in [6] it is argued that the series solution is rather complicated, and the ground impedance may be obtained directly from solving Pollaczek-Sunde's integral, numerically [7, 8].

The main objective of this paper, inspired by the research performed in [6], is to develop an efficient numerical algorithm for calculating ground- and sea-return impedances for power cables that guarantee absolute convergence, accuracy, and stability. This is achieved here by using the rapidly converging Wedepohl series for the low-frequency range and a trapezoidal integration rule for the high-frequency range.

Furthermore, to validate the here proposed numerical algorithm we test three different techniques commonly applied to numerically solve the Pollaczek-Sunde's integral [7, 8]. The first one is based on solving the Wedepohl series for the low-frequency range and the use of the closed-form approximation for the high-frequency range as directed in [6]. The second method consists in applying the Gauss-Kronrod quadrature [9] for the whole frequency range. The third methodology consists in applying the trapezoidal numerical integration routine directly to the unexpanded Pollaczek-Sunde's integral expression [7].

Finally, the proposed numerical algorithm is validated in a wide range of practical engineering application cases for studying cable transient overvoltages. This is achieved through the use of normalized dimensionless variables according to [10-11]. This validation shows that the proposed algorithm is accurate and computationally fast.

## II. GROUND- OR SEA- RETURN IMPEDANCES

### A. Fundamentals

The self and mutual earth-return impedances for a quasi-TEM<sub>z</sub> propagation mode for a cable system as the one depicted in Fig. 1 is calculated with [6-8]

---

Felipe Uribe and Pavel Zuniga are with the Electrical Engineering Graduate Program at The University of Guadalajara, Guadalajara Jalisco, México (e-mail: felipe.uribe@academicos.udg.mx).

Octavio Ramos-Leaños is with IREQ, Montreal, Canada (e-mail: ramos.octavio@ireq.com).

Paper submitted to the International Conference on Power Systems Transients (IPST2023) in Thessaloniki, Greece, June 12-15, 2023.

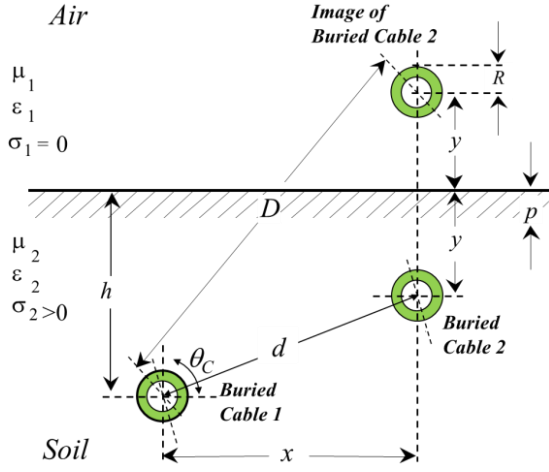


Fig. 1. Geometry of the underground system

$$Z_g(\omega) = \frac{j\omega\mu}{2\pi} \int_{-\infty}^{\infty} \left[ \frac{e^{-|y+h|\sqrt{\alpha^2+1/p^2}}}{|\alpha| + \sqrt{\alpha^2+1/p^2}} + \frac{e^{-|y-h|\sqrt{\alpha^2+1/p^2}} - e^{-|y+h|\sqrt{\alpha^2+1/p^2}}}{2\sqrt{\alpha^2+1/p^2}} \right] e^{j\alpha x} d\alpha \quad (1a)$$

where  $\alpha$  is the integration constant,  $\omega$  represents the angular frequency (in rad/s),  $\mu$  corresponds to the magnetic permeability (H/m) of the soil, and  $p$  is the complex depth considering displacement currents as given by [10].

$$p = 1/\sqrt{j\omega(\sigma + j\omega\epsilon_0\epsilon_r)\mu} \quad (1b)$$

where  $\epsilon_0 = 8.8541878176 \times 10^{-12}$  F/m is the vacuum permittivity and  $\epsilon_r$  is the material relative permittivity.

Substituting the second integral in (1a) through its equivalents Bessel functions, (1a) becomes

$$Z_g(\omega) = \frac{j\omega\mu}{2\pi} [K_0(D/p) - K_0(d/p) + J_{Poll}] \quad (2)$$

where

$$J_{Poll} = (I_2 - 2I_3 + I_4)p^2 \quad (3a)$$

with,

$$I_2 = \int_{-\infty}^{\infty} \sqrt{\alpha^2+1/p^2} \cdot e^{-(h+y)\sqrt{\alpha^2+1/p^2}} e^{j\alpha x} d\alpha \quad (3b)$$

$$I_3 = \int_0^{\infty} \alpha e^{-(h+y)\sqrt{\alpha^2+1/p^2}} e^{j\alpha x} d\alpha \quad (3c)$$

$$I_4 = \int_{-\infty}^{\infty} \alpha e^{-(h+y)\sqrt{\alpha^2+1/p^2}} e^{j\alpha x} d\alpha \quad (3d)$$

where the physical parameters  $x$ ,  $y$ ,  $h$ ,  $D$  and  $d$  are distances between conductors as shown in Fig.1.

The solution for  $I_2$  (3b) and  $I_4$  (3d) is given by

$$I_2 = \frac{2(h+y)^2}{D^2 p^2} K_2(D/p) + \frac{2[(h+y)^2 - x^2]}{D^3 p} K_1(D/p) \quad (4a)$$

$$I_4 = \frac{2jx(h+y)}{D^2} K_2(D/p) \quad (4b)$$

where  $K_1$  and  $K_2$  represent the modified Bessel functions of the first and second order, respectively. For  $I_3$ , the solution is given by [6, 7]

$$\begin{aligned} I_3 &= \frac{1}{D^2 p^2} \int_{(h+y)/D}^{\infty} [(h+y)^2 - x^2] t e^{-Dt/p} dt + \dots \\ &\dots + \frac{jx(h+y)}{D^2 p^2} \int_1^{\infty} \left[ \frac{1}{\sqrt{t^2-1}} + 2\sqrt{t^2-1} \right] e^{-Dt/p} dt + \dots \\ &\dots + \frac{x(h+y)}{D^2 p^2} \int_{(h+y)/D}^1 \left[ 2\sqrt{1-t^2} - \frac{1}{\sqrt{1-t^2}} \right] e^{-Dt/p} dt \end{aligned} \quad (4c)$$

The first integral in (4c) can be easily evaluated by traditional quadrature routines; the second integral is equivalent to  $K_2(D/p)$ , which can be approximated through polynomial series. In [6] it is proposed to evaluate the third integral of (4c) by a series expansion of the exponential function and then to integrate it term-by-term to obtain  $S_{ser}(D/p, |x|, \ell)$ , where the sum of cables depth is  $\ell=h+y$ .

Substituting the solution of each integral in (4c) we obtain

$$\begin{aligned} I_3 &= \frac{[(h+y)^2 - x^2]}{D^4} [1 + (h+y)/p] e^{-(h+y)/p} + \dots \\ &\dots + \frac{jx(h+y)}{D^2} K_2(D/p) + \dots \\ &\dots + \frac{x(h+y)^2}{D^2 p^2} S_{ser}\left(\frac{D}{p}, |x|, \ell\right) \end{aligned} \quad (4d)$$

The study of the numerical behavior of the component  $S_{ser}$ , which corresponds to the series solution in (4d), is analyzed in detail in the following sections.

### B. Wedepohl Series solution

Despite some typographical errors in [6] regarding the converging series,  $S_{ser}$  can be split up into four terms

$$S_{ser}\left(\frac{D}{p}, |x|, \ell\right) = S_1 + S_2 + S_3 + S_4 \quad (5)$$

$S_1$  to  $S_4$  are displayed here differently than in [6] for clarity of programming implementation. For instance, an analysis of  $S_1$ , given by (6a), reveals that the leading terms  $1/k(k+2)!$  and  $(D/p)^{k+2}$ ,  $k=2, 3, \dots$ , can be stored in two separate vectors which can be used as required. In addition, the telescopic nesting nature of the series solution remaining terms can be observed in (6)-(9).

As a programming example, a pseudo-code (based on MATLAB<sup>®</sup> notation [12]) has been added after the first term, given by (6a); for the second, third, and fourth terms, very similar pseudo-codes can be generated.

It is noted that the aforementioned leading terms are frequency dependent whereas the nested terms depend only on the geometry of the cable system.

### First series term $S_1$

$$\begin{aligned}
 S_1 = & \left\{ \theta - \frac{\ell \cdot |x|}{D^2} + \dots \right. \\
 & \dots + \frac{1}{2(2!)} \left( \frac{D}{p} \right)^2 \left\{ \frac{\ell \cdot |x|^3}{D^4} + \frac{1}{2} \left( \theta - \frac{\ell \cdot |x|}{D^2} \right) \right\} + \dots \\
 & \dots + \frac{1}{3(4!)} \left( \frac{D}{p} \right)^4 \left\{ \frac{\ell^3 \cdot |x|^3}{D^6} + \frac{3}{4} \left[ \frac{\ell \cdot |x|^3}{D^4} + \frac{1}{2} \left( \theta - \frac{\ell \cdot |x|}{D^2} \right) \right] \right\} + \dots \\
 & \dots + \frac{1}{4(6!)} \left( \frac{D}{p} \right)^6 \left\{ \frac{\ell^5 \cdot |x|^3}{D^8} + \frac{5}{6} \left[ \frac{\ell^3 \cdot |x|^3}{D^6} + \frac{3}{4} \left[ \frac{\ell \cdot |x|^3}{D^4} + \frac{1}{2} \left( \theta - \frac{\ell \cdot |x|}{D^2} \right) \right] \right] \right\} + \dots \\
 & \dots + \frac{1}{5(8!)} \left( \frac{D}{p} \right)^8 \left\{ \frac{\ell^7 \cdot |x|^3}{D^{10}} + \frac{7}{8} \left[ \frac{\ell^5 \cdot |x|^3}{D^8} + \frac{5}{6} \left[ \frac{\ell^3 \cdot |x|^3}{D^6} + \frac{3}{4} \left[ \frac{\ell \cdot |x|^3}{D^4} + \frac{1}{2} \left( \theta - \frac{\ell \cdot |x|}{D^2} \right) \right] \right] \right] \right\} + \dots \right\}
 \end{aligned} \quad (6a)$$

### Pseudo-code for $S_1$

$$\begin{aligned}
 & \text{factor\_1} = \theta - \frac{\ell \cdot |x|}{D^2}; \\
 & \text{for } k = 1 : N \\
 & \quad \text{factor\_1}(k) = \left( \frac{2k-1}{2k} * \text{factor\_1}(k) + \ell^{(2k-1)} \cdot \frac{|x|^3}{D^{2(k+1)}} \right); \\
 & \quad \text{Coef\_1}(k) = \frac{1}{(k+1) \cdot \text{factorial}(2k)} \left( \frac{D}{p} \right)^{2k}; \\
 & \text{end} \\
 & \text{term\_1} = (\text{factor\_1} * \text{Coef\_1}) + \left( \theta - \frac{\ell \cdot |x|}{D^2} \right);
 \end{aligned} \quad (6b)$$

### Second series term $S_2$

$$\begin{aligned}
 S_2 = & - \left\{ \frac{2}{3(1!)} \left( \frac{D}{p} \right) \left\{ \frac{|x|^3}{D^3} + \dots \right. \right. \\
 & \dots + \frac{2}{5(3!)} \left( \frac{D}{p} \right)^3 \left\{ \frac{\ell^2 \cdot |x|^3}{D^5} + \frac{2}{3} \left[ \frac{|x|^3}{D^3} \right] \right\} + \dots \\
 & \dots + \frac{2}{7(5!)} \left( \frac{D}{p} \right)^5 \left\{ \frac{\ell^4 \cdot |x|^3}{D^7} + \frac{4}{5} \left[ \frac{\ell^2 \cdot |x|^3}{D^5} + \frac{2}{3} \left[ \frac{|x|^3}{D^3} \right] \right] \right\} + \dots \\
 & \dots + \frac{2}{9(7!)} \left( \frac{D}{p} \right)^7 \left\{ \frac{\ell^6 \cdot |x|^3}{D^9} + \frac{6}{7} \left[ \frac{\ell^4 \cdot |x|^3}{D^7} + \frac{4}{5} \left[ \frac{\ell^2 \cdot |x|^3}{D^5} + \frac{2}{3} \left[ \frac{|x|^3}{D^3} \right] \right] \right] \right\} + \dots \\
 & \dots + \frac{2}{11(9!)} \left( \frac{D}{p} \right)^9 \left\{ \frac{\ell^8 \cdot |x|^3}{D^{11}} + \frac{8}{9} \left[ \frac{\ell^6 \cdot |x|^3}{D^9} + \frac{6}{7} \left[ \frac{\ell^4 \cdot |x|^3}{D^7} + \frac{4}{5} \left[ \frac{\ell^2 \cdot |x|^3}{D^5} + \frac{2}{3} \left[ \frac{|x|^3}{D^3} \right] \right] \right] \right] \right\} + \dots \right\}
 \end{aligned} \quad (7)$$

### Third series term $S_3$

$$\begin{aligned}
 S_3 = & - \left\{ \theta + \dots \right. \\
 & \dots + \frac{1}{2(2!)} \left( \frac{D}{p} \right)^2 \left\{ \frac{\ell \cdot |x|}{D^2} + \theta \right\} + \dots \\
 & \dots + \frac{1}{4(4!)} \left( \frac{D}{p} \right)^4 \left\{ \frac{\ell^3 \cdot |x|}{D^4} + \frac{3}{2} \left[ \frac{\ell \cdot |x|}{D^2} + \theta \right] \right\} + \dots \\
 & \dots + \frac{1}{6(6!)} \left( \frac{D}{p} \right)^6 \left\{ \frac{\ell^5 \cdot |x|}{D^6} + \frac{5}{3} \left[ \frac{\ell^3 \cdot |x|}{D^4} + \frac{3}{2} \left[ \frac{\ell \cdot |x|}{D^2} + \theta \right] \right] \right\} + \dots \\
 & \dots + \frac{1}{8(8!)} \left( \frac{D}{p} \right)^8 \left\{ \frac{\ell^7 \cdot |x|}{D^8} + \frac{7}{4} \left[ \frac{\ell^5 \cdot |x|}{D^6} + \frac{5}{3} \left[ \frac{\ell^3 \cdot |x|}{D^4} + \frac{3}{2} \left[ \frac{\ell \cdot |x|}{D^2} + \theta \right] \right] \right] \right\} + \dots \right\}
 \end{aligned} \quad (8)$$

### Fourth series term $S_4$

$$\begin{aligned}
 S_4 = & + \left\{ \frac{1}{1(1!)} \left( \frac{D}{p} \right) \left\{ \frac{|x|}{D} + \dots \right. \right. \\
 & \dots + \frac{1}{3(3!)} \left( \frac{D}{p} \right)^3 \left\{ \frac{\ell^2 \cdot |x|}{D^3} + \frac{2}{1} \left[ \frac{|x|}{D} \right] \right\} + \dots \\
 & \dots + \frac{1}{5(5!)} \left( \frac{D}{p} \right)^5 \left\{ \frac{\ell^4 \cdot |x|}{D^5} + \frac{4}{3} \left[ \frac{\ell^2 \cdot |x|}{D^3} + \frac{2}{1} \left[ \frac{|x|}{D} \right] \right] \right\} + \dots \\
 & \dots + \frac{1}{7(7!)} \left( \frac{D}{p} \right)^7 \left\{ \frac{\ell^6 \cdot |x|}{D^7} + \frac{6}{5} \left[ \frac{\ell^4 \cdot |x|}{D^5} + \frac{4}{3} \left[ \frac{\ell^2 \cdot |x|}{D^3} + \frac{2}{1} \left[ \frac{|x|}{D} \right] \right] \right] \right\} + \dots \\
 & \dots + \frac{1}{9(9!)} \left( \frac{D}{p} \right)^9 \left\{ \frac{\ell^8 \cdot |x|}{D^9} + \frac{8}{7} \left[ \frac{\ell^6 \cdot |x|}{D^7} + \frac{6}{5} \left[ \frac{\ell^4 \cdot |x|}{D^5} + \frac{4}{3} \left[ \frac{\ell^2 \cdot |x|}{D^3} + \frac{2}{1} \left[ \frac{|x|}{D} \right] \right] \right] \right] \right\} + \dots \right\}
 \end{aligned} \quad (9)$$

## III. ANALYSIS OF SERIES CONVERGENCE

### A. Wedepohl Series vs Trapezoidal Integration

Consider as a test case the three phase underground cable circuit described in [6] and shown here in Fig. 2. Each cable is buried at a 0.75 m depth and consists of a nucleus as a main conductor and a metallic sheath insulated with an extruded polymer and it is surrounded by a soil with a resistivity of 20  $\Omega\text{m}$ . The cable data is available in Fig. 11a.

As a first evaluation, we implemented the series solution  $S_{ser}$  given in (5) using 100 frequency samples uniformly spaced from 1 Hz to 10 MHz.

In a second evaluation, we applied the trapezoidal numerical integration to the third integral term of (4c) to the aforementioned frequency samples, labeled as  $S_{int}$ , taking an arbitrary integration time-step of  $1 \times 10^{-4}$ .

The behavior of both sets of solutions  $S_{ser}$  (in gray dashed lines) and  $S_{int}$  (in blue continuous dotted lines) is shown in Fig. 3 for its real and imaginary components.

The effect of varying the number of terms ( $N$ ) in the series solution  $S_{ser}$ , can be appreciated in the same figure for  $N = 1$  to  $N = 4$ , evidencing a rapid convergence with respect to the trapezoidal numerical solution  $S_{int}$ .

From Fig. 3 it can be noted that in practice the cut-off frequency convergence criterion of  $|D/p| > 2$  for  $N > 4$   $S_{ser}$  series terms can be acceptable in comparison to  $S_{int}$ . However, after several numerical evaluations, we have noticed that using more than four  $N$  terms did not meaningfully change the results of  $S_{ser}$ , which obeys to the theory of convergence of a series solution around a given point [9].

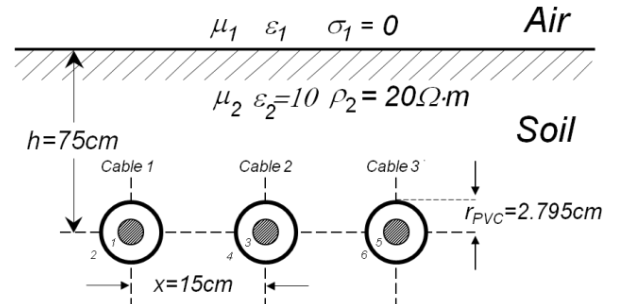


Fig. 2. Underground cable transmission system described in [6].

### B. Ratio Test

The uniform convergence of a sequence of partial sums (or of a series solution set  $S_n$ ) can be estimated using the following ratio test for  $n = 1, 2, 3$ , and 4 of the sequences [9]

$$\lim_{k \rightarrow \infty} \left| \frac{S_{n_{k+1}}}{S_{n_k}} \right| < 1 \quad (10)$$

The results of applying (10) to each of the series sequences of (6a), (7), (8) and (9) are shown in Fig. 3b with different colors and markers. From this test one can observe the smooth behavior of the four sets of curves of  $S_n$  tending uniformly to  $S_{ser}$ , which indicates a uniform convergence as indicated in [9].

### C. Proposed Numerical Algorithm

The four sequences (6a), (7), (8) and (9) of the series solution  $S_{ser}$  are in good agreement with the trapezoidal integration technique  $S_{int}$  when the number of series terms  $N \geq 4$  for  $|D/p| < 2$ , as can be observed from Fig. 3a using the test case from [6] and reproduced in Fig. 2.

The series  $S_{ser}$  in Fig. 3a give accurate results with very low computational expense up to  $D/|p| \approx 2$ , and therefore it is proposed here to be used as a criterion to switch between the series solution  $S_{ser}$  and the numerical integration  $S_{int}$ .

This criterion contrasts with the one proposed in [6, 8, 10, 11], where  $D/|p| < 0.25$  is used to switch between a series based and a closed-form solution of (2) [6].

The numerical procedure applied to calculate the ground-return impedances of the underground cable system shown in Fig. 2 is general. This means that it can also be extended to a broad range of practical application cases.

## IV. WIDE RANGE GROUND-IMPEDANCE DATA

To synthesize the electromagnetic transients of the cable system shown in Fig. 2 one has to use (1a) to calculate the ground-return impedances of the current loops formed inside each cable, as well as between near and far cables with respect to ground [11]. The geometrical distances (radii of the conductors and cables depth) and the media properties (resistivity of conductors, dielectric insulation permittivity, and magnetic permeability) of the system have to be measured or estimated. However, there are cases when it is impractical or very difficult to measure or obtain the necessary data to perform a transient study of an electrical equipment or system. On the other hand, the nameplate data that many manufacturers usually provide are only for 60 Hz.

Thus, in this section a wide range solution of  $J_{poll}$ , in (2), to calculate ground-return impedances for several practical cases which can also be used as a benchmark or as a look up-table is presented. Furthermore, the results can be used to assess the accuracy of any other ground-impedance solution method or formula [10].

Consider the following normalized dimensionless parameter definitions inspired from Carson's theory [13] for wave propagation in transmission lines shown in Fig. 4 and are expressed by [8, 13]:

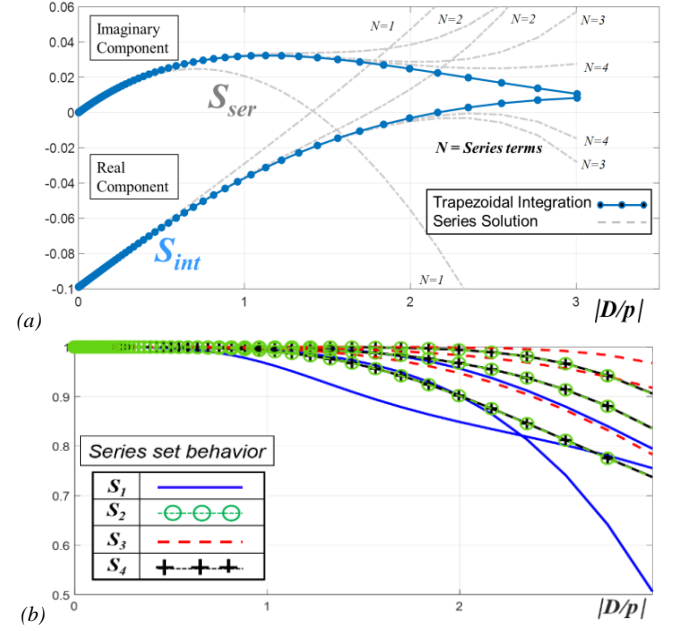


**Fig. 3.** Wedepohl series convergence test. (a) Convergence of series solution and trapezoidal integration with respect to the number of terms. (b) Ratio test.

$$\xi = \frac{y+h}{|p|}, \quad \eta = \frac{x}{y+h} \quad \text{and} \quad \chi = \frac{y-h}{y+h} \quad (11a)$$

After some mathematical manipulations, we obtain the wide-range representation of (2) in terms of (11a) as [8]

$$\underline{Z}_{Ground} \left( \frac{2\pi}{\omega\mu_0} \right) = j \cdot \left[ K_0(\sqrt{j} \cdot \xi \sqrt{\chi^2 + \eta^2}) - K_0(\sqrt{j} \cdot \xi \sqrt{1 + \eta^2}) + J_{poll}(\xi, \eta) \right] \quad (11b)$$

where now the term  $J_{poll}$  has been transformed into the following normalized parameters version of the Pollaczek-Sunde's integral [7, 8]

$$J_{poll}(\xi, \eta) = 2 \int_0^\infty \frac{\exp\left[-\xi \sqrt{u^2 + j}\right]}{|u + \sqrt{u^2 + j}|} \cos(u \cdot \xi \eta) du \quad (11c)$$

where the variable change  $\alpha = u/|p|$  used in (1a) is also used here to obtain (11c). Moreover, the transformation to normalized parameters is of general applicability, for instance, consider the following closed-form expression derived by Wedepohl from the series expansion [6]

$$\underline{Z}_{Ground} = \frac{j\omega\mu_0}{2\pi} \cdot \left[ -\log(\gamma d/2p) + \frac{1}{2} - \frac{2(h+y)}{3p} \right] \quad (11d)$$

Which in the normalized form (11d) now becomes a function of  $\xi$ ,  $\chi$ , and  $\eta$ , as follows [8]

$$\underline{Z}_{Ground} \left( \frac{2\pi}{\omega\mu_0} \right) = j \cdot \left[ -\log\left(\gamma \sqrt{j} \cdot \xi \sqrt{\chi^2 + \eta^2} / 2\right) + \frac{1}{2} - \frac{2}{3} \sqrt{j} \cdot \xi \right] \quad (11e)$$

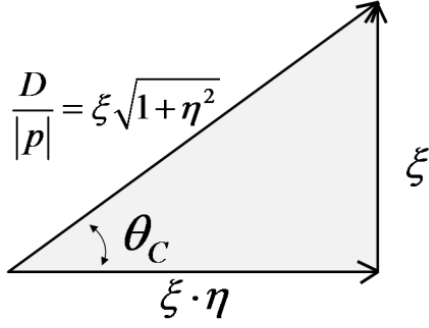


Fig. 4. Vector data normalization and research basis according to Carson's theory for calculating ground-wave return-impedances [13].

The physical and normalized variable ranges are presented in Table I.

TABLE I  
PHYSICAL AND NORMALIZED DATA

Description	Physical variables	Normalized parameters
Conductor depth (m)	$0.5 < h, y < 100$	
Distance between cables (m)	$0 < x < 500$	
Conductivity of soil (S/m)	$10^{-4} < \sigma < 1$	
Angular frequency (rad/s)	$2\pi < \omega < 2\pi \times 10^9$	
Defined in (11a)		$10^{-6} < \xi < 10^2$
Defined in (11a)		$10^{-3} < \eta < 10^4$
Defined in (11a)		$0 < \chi < 1$

Fig. 5 presents the numerical solution of  $J_{Poll}(\xi, \eta)$ , given by (11c). This solution was obtained applying the here proposed numerical algorithm of section 3-C, taking 100 samples for  $\xi$  and 10 samples for  $\eta$ , logarithmically spaced.

As can be seen from these figures, there are no numerical oscillations present in the curves for the 1,000 samples, which were computed in less than 1 s. For this reason, the numerical algorithm presented here is taken as a reference to validate the numerical accuracy and processing time of other numerical methods and formulas to approximate the Pollaczek-Sunde integral for the calculation of ground-return impedances.

## V. COMPUTATIONAL PERFORMANCE

The wide range solution data shown in Fig. 5 was obtained with the here proposed numerical algorithm that uses the convergent series in (5) combined with the trapezoidal integration of the third integral of (4c).

The here proposed algorithm is used as a reference to test the trapezoidal integration method applied to the third integral of (4c), the Wedepohl series that uses convergent series for the low-frequency range and the closed-form solution of (11d) or (11e) for the high-frequency range [6], and the Gauss-Kronrod quadrature method applied to (11c) using the default absolute tolerance of  $1 \times 10^{-10}$  (with a double precision format).

Table II resumes the RMS error and the computer processing time for each case, choosing three different values of the normalized variable  $\eta$  taken from the table curves in Fig. 5.

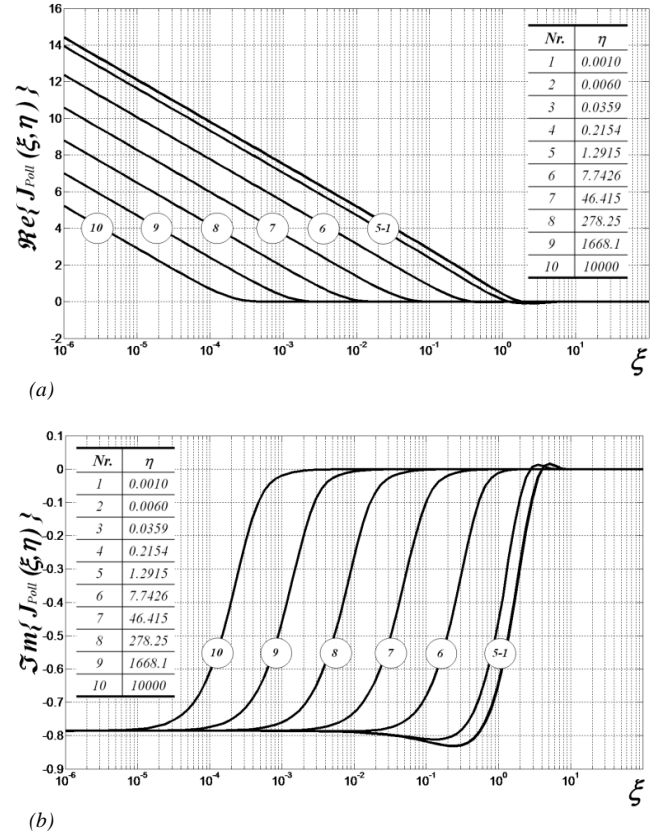


Fig. 5. Numerical algorithm wide range solution data of  $J_{Poll}(\xi, \eta)$ .  
(a) Real component, (b) Imaginary component.

The results in Table II were obtained running MATLAB® r7.8 [12] on a 3.4 GHz processor with 8 GB of RAM. Windows 7 Professional 64 bits, and an Intel Core i7-2600 CPU.

As can be seen in Table II, the processing time for the Gauss-Kronrod method is larger than for any other method tested here (much larger for  $\eta_{10}$ ), as expected. The Wedepohl series processing times are comparable to the trapezoidal routine and the numerical algorithm proposed here; however, the RMS error increases for large values of  $\eta$ . This is due to the “weak” switching criterion between the series and the closed-form approximation in [6].

## VI. TRANSIENT RESPONSE OF UNDERGROUND CABLE SYSTEM

The transient response of the underground cable system shown in Fig. 2, with 500 m length, is synthesized here through the Numerical Laplace Transform (NLT) [11]. This is obtained with a unit-step voltage source injected into the core of cable 1 at the sending-end of the system. The voltage at the receiving-end is shown in Fig. 6a for the energized-core, whereas the induced voltages for cores 3 and 5, and sheaths 2, 4, and 6 are shown in Fig. 6b. The cable data for this numerical experiment is available in Fig. 11a of the Appendix.

It should be mentioned here that, when the core of cable 1 is energized, the magnitude of the induced voltages and circulating currents becomes smaller as the ground-loop distances through the ground increases.

In these types of cases, the accuracy in the ground-return impedance calculation is of high importance to identify

electromagnetic couplings and interferences with any other transmission or communication system in the vicinity [13, 14].

The transient responses corresponding to Fig. 6 have also been obtained with: 1) the Gauss-Kronrod quadrature applied to (11c), 2) the EMTP methodology [10], and 3) the Wedepohl series [6].

In the EMTP-type software, the evaluation of the Pollaczek's integral is replaced by using the Carson's integral as indicated by Professor A. Ametani [10, 13, 14].

Fig. 7 depicts the relative differences for the induced voltages formed between the loop of cable 1 core-1 and the sheath-6 of cable 3, calculated with

$$\varepsilon_{rel}^{\%} = \left| 1 - \frac{func_{approx}}{\max(func_{exact})} \right| \times 100 \quad (12)$$

where  $func_{exact}$  is the value taken as a reference and corresponds to the here proposed algorithm, and  $func_{approx}$  are the aforementioned approximations to calculate ground-return impedances.

TABLE II  
CPU PROCESSING TIME RMS ERROR

		Test methodology			
		Trapezoidal rule	Numerical algorithm	Wedepohl series	Direct Gauss-Kronrod
$\eta_1$	CPU time (s)	0.06240040	0.07800050	0.09360059	0.3588020
	rms error	0.00001041	base	0.03823930	0.0000030
$\eta_5$	CPU time (s)	0.07800050	0.07800050	0.07800050	0.3900024
	rms error	0.00429982	base	0.04447860	0.0006413
$\eta_{10}$	CPU time (s)	0.06240040	0.09360060	0.09360060	6.3024403
	rms error	0.00000092	base	0.20897890	0.0071932

## VII. TRANSIENT RESPONSE OF SUB-SEA CABLE SYSTEM

In this section, the transient step-responses for the sub-sea cable system with 1 km length and 60 m depth, shown in Fig. 8, are synthesized through the NLT using the here proposed ground-sea-return impedances numerical algorithm.

The transient step response of the core at the remote-end of the energized cable is shown in Fig. 9a, whereas the induced voltages at the remote-end of cable cores 2-3 and cable sheaths 4-5-6 are shown in Fig. 9b. The cable data for this numerical experiment is available in Fig. 11b in the Appendix.

According to the observed behavior of induced voltages in Fig. 6b and Fig. 9b, one can observe that the voltage magnitudes of cores and sheaths of the sub-sea power cables are magnified compared to the underground case, probably due to the smaller thickness of the interlayers between conductors and dielectrics. This also means that the diameter of the sea-cable nucleus is more than two times greater than the one used in the underground cable distribution system. In addition, the sea-resistivity plays a very important role in the solution of sub-sea cable projects.

There are many research challenges in finding a general and practical frequency-dependent ground resistivity equation that can consider the resistive and displacement currents regions.

It can be observed from the results that transient overvoltages are highly sensitive to the ground-sea-return impedances.

Fig. 7 and Fig. 10 shows the relative differences in the induced transient voltages for the loop formed between the energized core and sheath of the far-cable, for both the underground and sub-sea cable systems testing the numerical algorithms. The relative differences are calculated with the three aforementioned methodologies. From these methods, the one proposed by Ametani [14] presented the best numerical performance in accuracy and computer processing time.

## VIII. CONCLUSIONS

The Wedepohl series formulation to approximate the ground-sea-return impedance, as given by the Pollaczek-Sunde equation, has been implemented and numerically studied in this paper. An accurate and robust numerical algorithm to reliably solve the Wedepohl series and thus reliably compute the ground-sea-return impedance has been proposed and analyzed here. It has been demonstrated that the proposed solution can be applied to a wide range of practical cases and can be used to assess other numerical methods such as direct numerical integrations, closed-form approximations or automatic quadrature rules. It has been shown via transient analysis that the proposed algorithm is capable of handling underground cable systems as well as subsea cable systems that present very low resistivities and large depths.

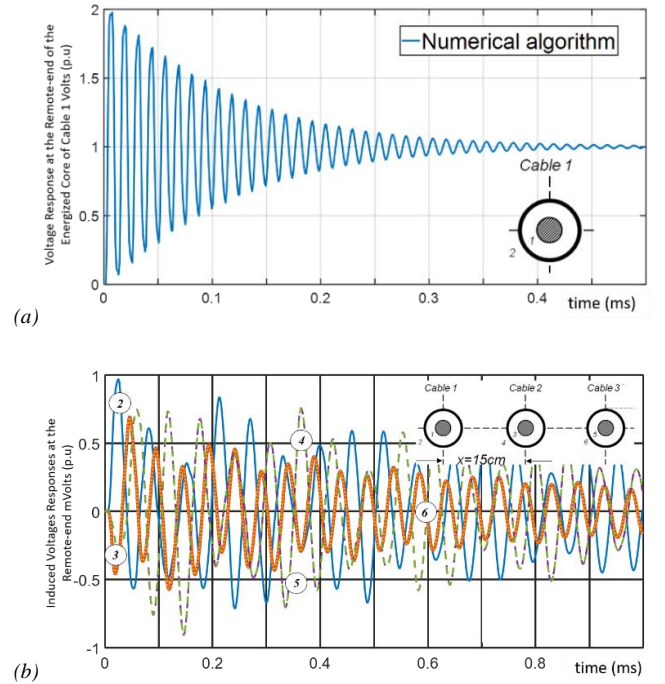


Fig. 6. Voltage step-responses at the receiving end. (a) Energized core of cable 1. (b) Induced transient voltages (in mV) at cores 3 and 5 and sheaths 2, 4, and 6.

From the obtained results, it is noticed that a precise calculation of such impedances is needed to obtain accurate time-domain transient responses which are highly sensitive to physical and geometrical variables and media properties such as ground or seawater resistivity.

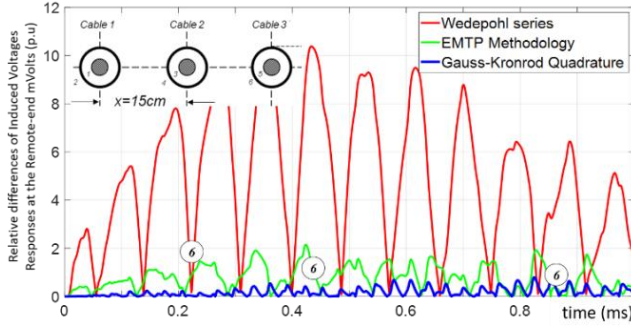


Fig. 7. Relative differences for induced voltage responses formed between the loop of cable core-1 and the cable sheath-6.

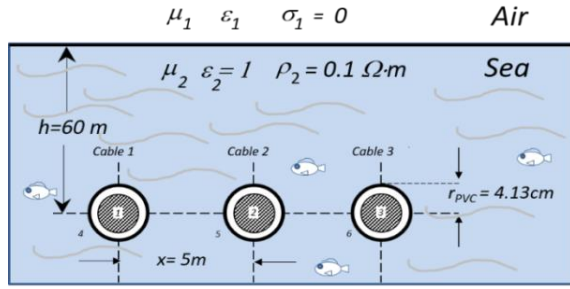


Fig. 8. Sub-sea power cable prototype transmission system.

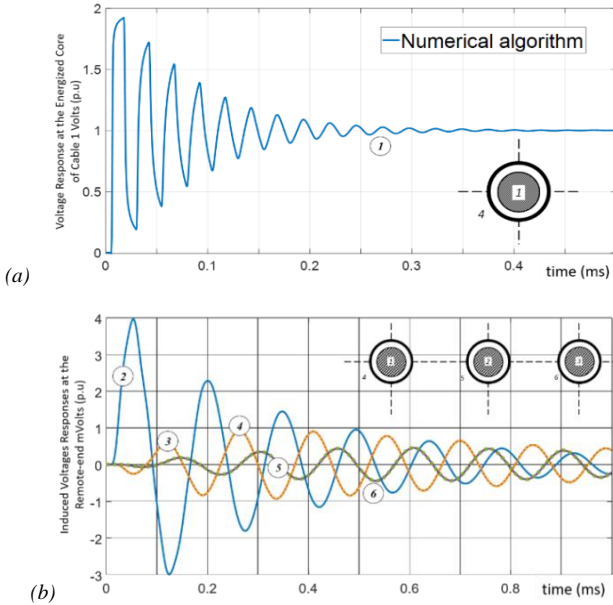


Fig. 9. Voltage step-responses at the receiving-end of the sub-sea cable system test. (a) Energized core of cable 1. (b) Induced transient voltages in (mV) at cores 3 and 5 and sheaths 2, 4, and 6.

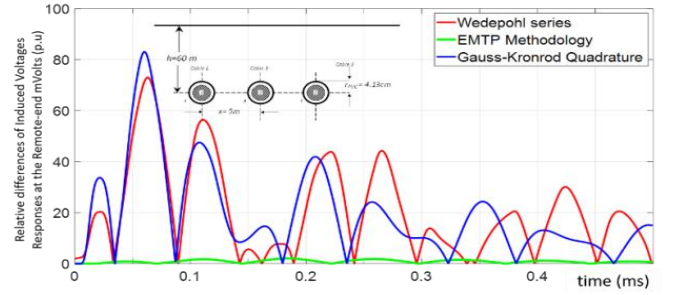


Fig. 10. Relative differences in the induced transient responses for the loop formed between cable core-1 and sheath-6.

## IX. APPENDIX

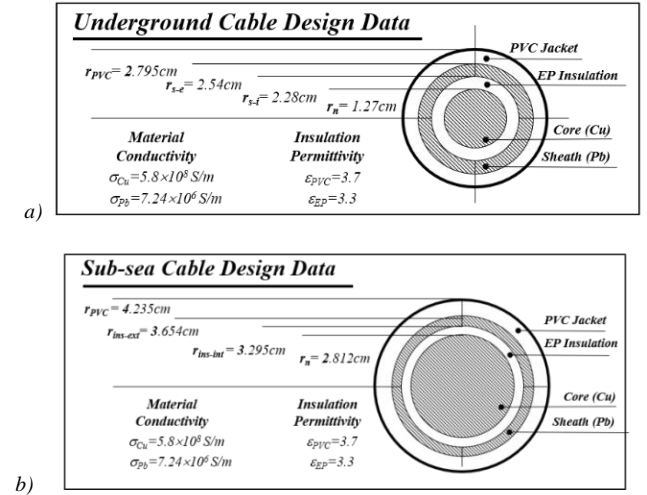


Fig. 11. Cable design data. a) Underground distribution electrical cable. b) Sub-sea power electrical prototype cable.

## X. REFERENCES

- [1] Global Change Data Lab and the Our World in Data team. <https://ourworldindata.org/>
- [2] T. A. Papadopoulos, D. A. Tsiamitros, and G. K. Papagiannis, "Impedances and admittances of underground cables for the homogeneous earth case," *IEEE Trans. Power Del.*, vol. 25, no. 2, pp. 961-969, 2010.
- [3] A. P. C. Magalhães, J. C. L. V. Silva, A. C. S. Lima, and M. T. Correia de Barros, "Validation limits of quasi-tem approximation for buried bare and insulated cables," *IEEE Trans. Electromagn. Compat.*, vol. 57, no. 6, pp. 1690-1697, 2015.
- [4] H. Xue, A. Ametani, J. Mahseredjian, and I. Kocar, "Generalized formulation of earth-return impedance/admittance and surge analysis on underground cables," *IEEE Trans. Power Del.*, vol. 33, no. 6, pp. 2654-2663, 2018.
- [5] N. Duarte, A. De Conti, and R. Aliipo, "Assessment of ground-return impedance and admittance equations for the transient analysis of underground cables using a full-wave FDTD method," *IEEE Trans. Power Del.*, vol. 37, no. 5, pp. 3582-3589, 2022.
- [6] L. M. Wedepohl, *et al.*, "Transient analysis of underground power-transmission systems", *Proc. IEEE*, vol. 120, No. 2, pp. 253-260, February 1973.
- [7] F. Pollaczek, "Über das Feld einer unendlich langen wechselstromdurchflossenen Einfachleitung", *Electrische Nachrichten Technik*, Vol. 3, No. 9, pp. 339-360, 1926.
- [8] F. A. Uribe, J. L. Naredo, P. Moreno and L. Guardado, "Algorithmic evaluation of underground cable earth impedances," *IEEE Transactions on Power Delivery*, Vol. 19, No.1, pp.316-322, January 2004.

- [9] W. Kaplan, *Advanced Mathematics for Engineers*. Addison Wesley, 1981, chapter. 2.
- [10] W. Dommel, *Electromagnetic Transients Program Reference Manual (EMTP Theory Book)*, Prepared for Bonneville Power Administration, P.O. Box 3621, Portland, Ore., 97208, USA, 1986.
- [11] F. A. Uribe, J. L. Naredo, P. Moreno, L. Guardado, "Electromagnetic transients in underground transmission systems through the Numerical Laplace Transform", *International Journal of Electrical Power & Energy Systems*, Elsevier Science Ltd, September 2000.
- [12] MathWorks, MATLAB R2017. <https://www.mathworks.com>. (Accessed 3 December 2022).
- [13] J. R. Carson, "Wave propagation in overhead wires with ground return", *Bell Systems Tech. J.*, pp. 539-554, 1926.
- [14] A. Ametani, T. Yoneda, Y. Baba, and N. Nagaoka, "An investigation of earth-return impedance between overhead and underground conductors and its applications", *IEEE Transactions on Electromagnetic Compatibility*, Vol. 51, No.3, pp.860-867, August 2009.